



Mission Research Corporation

MRC/WDC-R-424

COMPARISON OF HELIX TWT SIMULATION USING 2-D PIC (MAGIC), 2-D MODAL (GATOR), AND 1-D MODAL (CHRISTINE) METHODS

David N. Smithe

May 1998

Technical Report

Prepared for: Naval Research Laboratory
Code 6841, Vacuum Electronics Branch
4555 Overlook Ave., SW
Washington, DC 20375

Contract No: N00014-96-C-2047
Amplifier Research

Prepared by: Mission Research Corporation
8560 Cinderbed Rd.
Suite 700
P. O. Box 8560
Newington, VA 22122-8560

19980601 075

DTIC QUALITY INSPECTED 3

DISTRIBUTION STATEMENT A

Approved for public release;
Distribution Unlimited

TABLE OF CONTENTS

ABSTRACT	ii
SECTION 1. OVERVIEW	1
SECTION 2. INFINITE B-FIELD COMPARISON	3
2.1 DRIVE CURVE	3
2.2 HARMONICS	5
2.3. NECESSITY OF HARMONICS	7
SECTION 3. BRILLOUIN B-FIELD COMPARISON.....	8
3.1 IMPORTANCE OF RADIAL MOTION	8
3.2 DRIVE CURVE	8
3.3 DETAILS OF SINGLE BRILLOUIN RUN	9
3.4 OUTLIER ELECTRON EFFECT IN GATOR	12
3.5 EMISSION CONDITION AND NONLAMINAR FLOW IN MAGIC.....	12
3.6 RADIAL SHEAR.....	13
SECTION 4. PPM B-FIELD COMPARISON	16
SECTION 5. ANALYSIS OF ACCURACY	20
5.1 ELECTROMAGNETIC / ELECTROSTATIC SEPARATION.....	20
5.2 MODAL METHOD BASED ON POTENTIALS	22
5.3 ACCURACY CHECK FOR THE MODAL METHODS	23
5.4 ACCURACY CHECK FOR THE PIC METHOD	25
SECTION 6. SUMMARY	27
REFERENCES	28

Comparison of Helix TWT Simulation using 2-D PIC (MAGIC), 2-D Modal (GATOR) and 1-D Modal (CHRISTINE) methods *

D.N. Smithe^(a), H. Freund^(b), T. M. Antonsen Jr.,^{(b),(c)} E. Zaidman
and B. Levush

*Code 6841, Vacuum Electronics Branch
Naval Research Laboratory, 4555 Overlook Ave., SW, Washington DC 20375
Tel. (202) 767-0037, Fax. (202) 767-1280, E-mail: levush@mmace.nrl.navy.mil*

ABSTRACT

(Paper presented at the 1998 Microwave Vacuum Electron Devices Conference.)

A series of comparisons between three different helix TWT design and simulation codes has been performed. The codes represent various different levels of approximation and speed. All codes utilize the sheath helix approximation. The 2-D PIC code, MAGIC, solves the Maxwell-Lorentz equations directly, in time, through simulations with large numbers of particles. Therefore, it is expected that the PIC code is capable of resolving the space-charge effects accurately. Unfortunately, because of long run times, it is difficult to perform many simulations with many different parameters in a timely manner, allowing a device to be designed and optimized numerically. The 2-D parametric code GATOR solves the envelope equation for the mode amplitude (hence the name "modal") of the electromagnetic field, and models the electron beam as an ensemble of rings of variable radius, making it much faster than the MAGIC code. However, the models to evaluate the DC and AC space-charge fields in GATOR are phenomenological, and typically less accurate over a wide range of parameters than in a PIC code. An important goal of the work reported here is to provide understanding of and possible improvement to the electrostatic model implemented in GATOR. The 1-D parametric code CHRISTINE is the fastest of the three codes, and it includes built-in parametric scan capability. Like GATOR it solves the envelope equation for the field amplitude in time and position, but it tracks only the axial particle motion. Its simple fixed disc model also allows for self-consistent calculation of the AC space-charge field. For a device whose electron beam is well confined by the radial focusing forces, CHRISTINE is able to reproduce accurately the performance of the device. Indeed, all three codes are in excellent agreement in the limit of a very strong solenoid magnetic field. Results of the comparison between MAGIC and GATOR for both a solenoid and PPM focusing cases will be discussed.

(*) This work is supported by the Office of Naval Research Laboratory. The computational work was partially supported by a grant of HPC time from the DoD HPC Center CWES

(a) Mission Research Corporation, Newington, VA

(b) Science Application Corporation, McLean, VA

(c) University of Maryland, College Park, MD

SECTION 1. OVERVIEW

A series of comparisons between three different helix TWT design and simulation codes has been performed. The codes represent various different levels of approximation, speed of execution, and simplicity of results. All codes utilize the sheath helix approximation. All codes are based on particle-pushing through the sheath helix fields to solve for the output power of the helix TWT.

The 2-D PIC code, MAGIC,¹ should have the best accuracy, especially in the area of space-charge effects, because of its faithful reproduction of the original Maxwell-Lorentz field equations. Unfortunately, MAGIC's run-time is long, and its output can be unwieldy to the uninitiated. This is a major hindrance to its use as a design tool.

The 2-D Modal code, GATOR,² retains 2-D particle kinematics, but solves for just the mode amplitude of the sheath helix traveling wave (hence the name "modal"), making it much faster than the MAGIC code, and hence better suited for a design tool. However, since the sheath helix traveling wave is divergence-free, this leaves the "electrostatic" component of the field unspecified. An important goal of the work reported here is to provide understanding of and possible improvement to the electrostatic model implemented in GATOR in order to faithfully reproduce the 2-D particle kinematics in both the solenoid and PPM scenarios. Indeed, the original impetus behind this investigation was an apparent high degree of particle losses to the helix in a situation where experimental results and MAGIC simulations indicated otherwise.³

The 1-D Modal code, CHRISTINE,⁴ (sometimes called TINI), also solves for the amplitude of the sheath helix traveling wave, and it is the fastest of the three codes. However, it tracks only the axial motion of the particles and assumes a rigid radial profile for the beam. This permits a clever and considerably more direct attack on the space-charge problem, and CHRISTINE has a more consistent space-charge model than GATOR. Unfortunately, the assumption of a rigid radial profile is costly, since in a real tube the beam tends to move outward in radius as it slows down. The increase in radius results in improved beam coupling to the helix as it slows down, an effect which is noticeable in both of the 2-D methods, but is absent from CHRISTINE.

The results of this study showed that in the infinite solenoid magnetic field limit, (e.g., no radial motion) all three codes are in excellent agreement on the power at the fundamental frequency, with MAGIC, GATOR, and CHRISTINE lying virtually on top of each other. In the linear growth regime, the power in the harmonics is also in rough agreement, with MAGIC consistently a little low in power. However, more obvious differences occurred in the power on the harmonics after saturation, with MAGIC in conflict with GATOR and CHRISTINE. The reason for this difference is unknown at this time, but one likely explanation is the neglect of grow-rate terms compared to the phase velocity term in the modal approximation, $\partial_z \rightarrow \omega/v_{ph}$.

Originally, when the infinite solenoid field was relaxed to the Brillouin value GATOR had beam losses. During the course of this work, GATOR was updated to provide an improved model for the electrons outside the nominal beam radius, e.g., "outlier" electrons, which seems to have cured this deficiency. MAGIC also shows some discrepancy of outer electron orbits in both the Brillouin flow and PPM scenarios. This discrepancy was traced to the fact that the particle charge and forces are assigned to

nearest grid locations, which results in the rounding-off of the charge density profile and the smoothing of the forces over the outer two cells of the beam profile. The effect is partially remedied with an appropriate reduction in the azimuthal velocity of the outer electrons, consistent with a smoothed profile.

In the Brillouin field, MAGIC and GATOR gave excellent agreement through saturation. After saturation, significant differences appeared, and seemed to indicate some remaining deficiency in the GATOR space-charge model, most likely due to some addition subtle inconsistency in radial factors. The problem seems to manifest itself first in the particle trajectories, which in turn affect their coupling to the RF. However, given the unsuitability of TWT's in the post-saturation regime, and the excellent agreement before saturation, this questionable post-saturation behavior does not present a problem for the use of GATOR in designing practical TWT's.

In a PPM field, the agreement between MAGIC and GATOR up to saturation was also excellent. At saturation, there was some departure of the two methods. However, the comparison was made difficult because of the inability of MAGIC to produce an ideal match to the PPM field at the beam emission point. Thus, there was larger scalloping in the MAGIC trajectories, and the obvious potential which that creates for causing divergence of the two results.

Based upon this study, the following recommendations are made. First, the 1-D modal method in CHRISTINE can be made much more accurate by adding a radial expansion model, if a suitable means of computing the radial expansion can be arrived at. Even a user-supplied radial expansion parameter would be highly useful. Second, the space-charge model in the 2-D modal method, GATOR, needs to plot an error quantity as a function of axial position, e.g., $|\nabla \cdot \epsilon \mathbf{E} - \rho|/\rho_0$. Both CHRISTINE and GATOR should track the validity of the modal approximation. These consistency checks would be very helpful to the user for determining accuracy of the model, without having to resort to PIC methods for verification. Third, the 2-D PIC method, MAGIC, needs built-in Brillouin and PPM emission models which are consistent with its finite-difference grid forces.

SECTION 2. INFINITE B-FIELD COMPARISON

The base test case for the comparisons in this paper are based upon the C-Band #8 tube built specifically for experimental comparison purposes by Northrop. The pertinent design parameters are:

Helix Length = 9.5758 cm,
Wall Radius = 2.794 mm,
Helix Radius = 1.2446 mm,
Helix Pitch = 0.80137 mm,
Helix Pitch (Angle) = 5.851 degrees,
Effective 2-D dielectric constant of the helix support rods = 1.75,

Frequency = 5.0 GHertz,
Nominal RF Input Power = 30 milliwatts,
RF Input Power Range = 0.1 – 100 milliwatts,

Beam Voltage = 3.00 kVolts,
Beam Current = 0.17 amps,
Beam Radius = 0.5 mm,
Beam Profile = Flat,
Brillouin Field = 0.94 kGauss uniform,

For the so-called infinite-B field comparisons, an actual field of 25 kG (= 20 times Brillouin) was used. In all runs at this field, there was no observable radial motion in either 2-D model. In GATOR, an initial condition of $m_{spac}=1$ was used. The proper cold-test behavior, e.g., dispersion and impedance, of the sheath helix element in each of the three methods has been widely studied, and verified.

2.1 DRIVE CURVE

Drive curves comparing all three methods are illustrated in Figures 2.1.1-2.1.3. All drive curves are represented with both log-log, and linear-linear scales. The log-log scale plot is useful for comparing the linear growth regime at low power levels. The linear-linear scale plot is necessary to compare the power levels at saturation. In addition, the drive curves are shown for three positions down the length of the tube, at 7 cm, 8 cm, and 9 cm.

In the linear growth regime, the initial slope on the log-log plots should be unity. All three codes show the initial unity slope. However, the 1-D modal method, CHRISTINE, shows an interesting power offset from the 2-D methods, which is apparent in all plots. This means that by the 7 cm position, the wave in CHRISTINE has grown slightly less, about 1 dB out of 37.5 dB gain, than that of the 2-D methods. This discrepancy remains unresolved, but is sufficiently small that it may be caused by any number of second-order effects, or possibly by some, as yet, undiscovered intrinsic difference between the 1-D and 2-D methods at the input injection point.

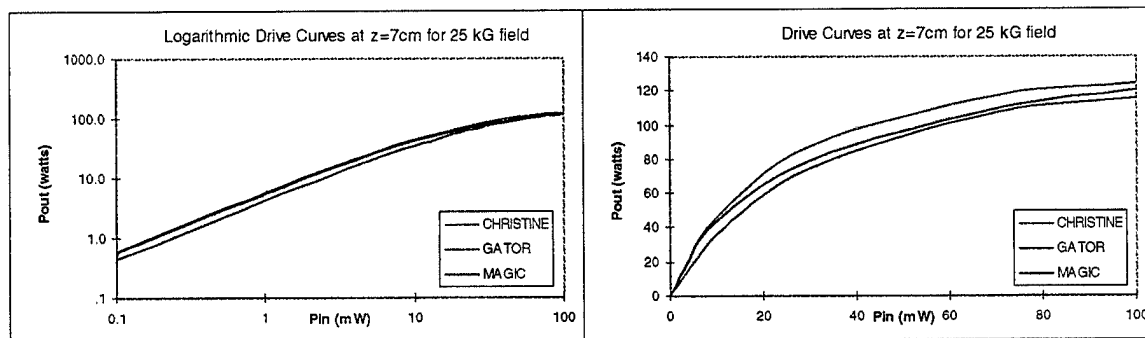


Figure 2.1.1 Infinite field drive curve comparison at 7 cm. Saturation occurs only at very high input power at or above 100 milliwatts. All methods agree across the range.

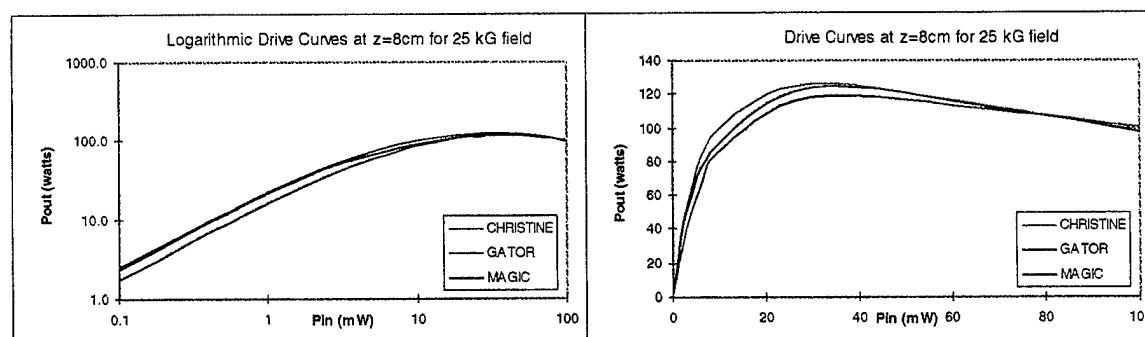


Figure 2.1.2 Infinite field drive curve comparison at 8 cm. Saturation occurs at the nominal 30 milliwatt input power. Excellent agreement across the range, even as the saturated power is decreasing in the 30–100 milliwatt range.

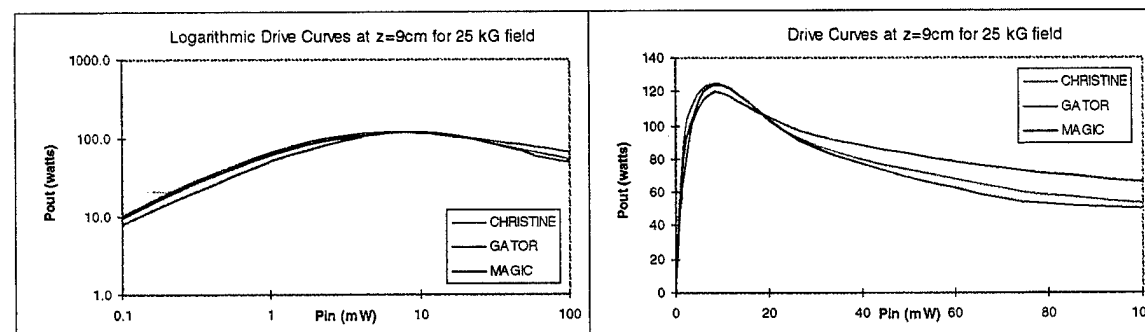


Figure 2.1.3 Infinite field drive curve comparison at 9 cm. Saturation occurs at about 8 milliwatts input power. The saturated power decreases by a factor of two from peak. 1-D modal, CHRISTINE shows a slightly lower decrease.

Saturation occurs at about 125 watts output power at all three locations. The input power required to achieve saturation is obviously less for the greater length locations, though. As the input power exceeds that necessary for saturation, the power is seen to

decrease, as expected from ballistic debunching. For the longest length at the highest input power, e.g., 9 cm at 100 milliwatts input, the post-saturation power predicted by the 2-D method, GATOR, is 15 watts higher, 65 vs. 50 watts, than the 1-D modal and 2-D PIC methods. There is frequent divergence in GATOR's post-saturation behavior throughout this study, and reasons for the differences are explored in later sections.

2.2 HARMONICS

A closer look at the power in the 1st harmonic shows that, despite the overall agreement in power levels between the codes, there are still some areas of systematic disagreement. Figure 2.2.1 shows the growth of the fundamental and harmonic powers for the nominal input power of 30 milliwatts. The most interesting feature is the dip in harmonic power, known as the "Whaley dip", which occurs at 7.8 cm in the 2-D PIC method, and 8.5 cm in the 1-D modal and 2-D modal methods. The dip is anticipated, and is due to the beam bunches, which travel at the phase velocity of the fundamental, eventually falling out of phase with the harmonic signal, which travels at a slightly different velocity, because of circuit dispersion.⁵ It is seen that the modal methods agree on the location and severity of the dip, while the 2-D PIC method shows a less severe dip, which occurs earlier. The exact reason for this interesting difference between the modal and PIC methods remains unknown, however, it is possible that approximations of the modal method, e.g., the neglect of terms involving the derivatives of the mode amplitudes, might account for the differences, as discussed in later sections. By way of counter argument, there is some experimental evidence which seems to be in closer agreement with the location and size of the dip as predicted by the modal methods.⁶ One way in which the PIC method might be subject to failure is the possible effect of boundary conditions and the presence of a small reflected wave component. It is even possible that the PIC and modal results might *both* be accurate, if for example, the difference was due to the fact that the PIC method illustrates all power flow, including the kinetic flux (see later sections), whereas the modal methods (and the experimental measurements) indicate only the power flow on the helix. Further research into this issue is obviously necessary.

The comparison of harmonics is complicated by an unfortunate failure of the 2-D PIC method to track the complete power evolution of the harmonic signal, as is evident in the figure. The 2-D PIC method suffers from having an absolute floor, below which it is incapable of diagnosing the power. This floor exists at 1 milliwatt for these runs, and seems to relate to the level of particle noise and the length of Fourier-transform time integral. It is believed that the origin of this floor is noise in the roughly 18 watts Poynting flow from the DC electric and magnetic fields of the beam; e.g., there is a 1 milliwatt particle noise component on top of the 18-watt DC power flow. There is no simple way to remove the noise since the 2-D PIC method does not separate DC and RF fields, instead all physics is present in a single field. Unfortunately, increasing particle number and increasing the length of the Fourier time integral both reduce particle noise at a very slow rate to have much impact on the problem.

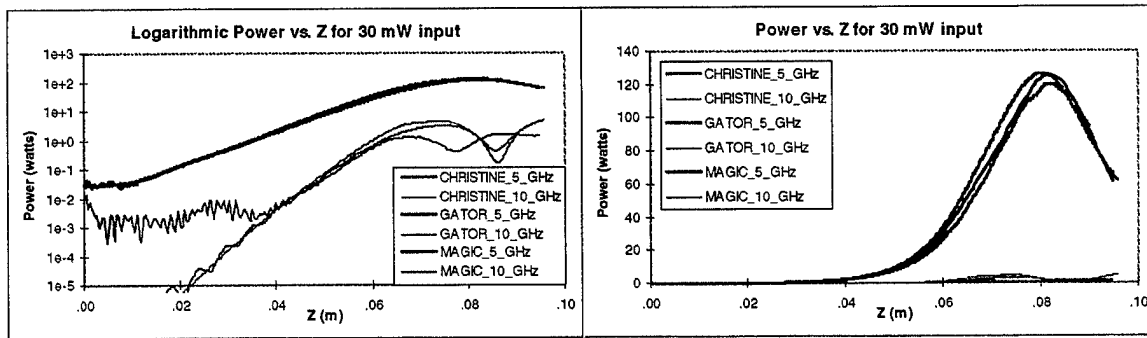


Figure 2.2.1 Growth of power in fundamental and harmonic vs. length down the tube for 30 milliwatts input power. An interesting difference between the PIC and modal methods is apparent in the harmonic power “dip” after saturation. The apparent floor in PIC power at 1 milliwatt is an artifact of a noise limitation on the power diagnostic.

Despite the low-power failings of the 2-D PIC power diagnostic, it is possible to compare the harmonic power in the latter part of the linear growth regime between 4 cm and 6 cm, where the agreement seems quite good between all three methods. The growth rate of the harmonic is expected to be twice that of the fundamental, e.g, 118 dB/cm for the harmonic as opposed to 58.8 dB/cm for the fundamental. The 1-D modal method holds closest to this growth rate, while the 2-D PIC method shows significant reduction in growth rate earlier than the other methods.

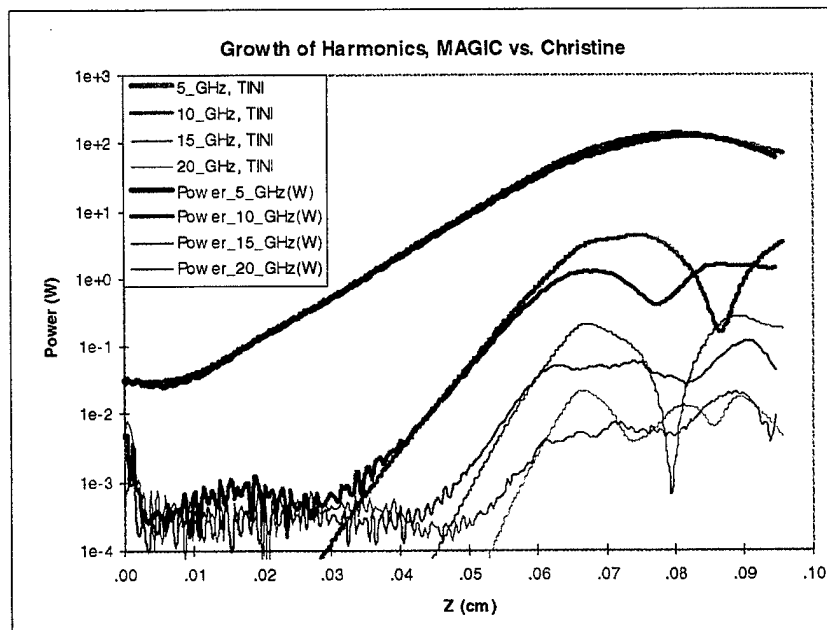


Figure 2.2.2 Comparison of 1-D modal and 2-D PIC harmonic growth. The differences in the behaviors of the power dips at saturation and the linear regime growth rates points to some fundamental area of difference between the physics of the modal and PIC methods.

The 1-D modal and 2-D PIC methods can be contrasted even more by looking at the higher harmonics. Figure 2.2.2 shows that the difference between the linear regime growth rates for the 1-D modal and 2-D PIC methods gets larger for higher harmonic numbers. In addition, the behavior of the power dips at saturation is also markedly different between the methods. It is tempting to search for some physical effect which could simultaneously cause the 2-D PIC method to saturate the harmonic growth rates earlier and smooth out the effects of the power dip. To date, no such physical effect has been positively identified.

2.3. NECESSITY OF HARMONICS

Inclusion of harmonics is a necessity for any helix TWT which comes within about 5 dB of saturation. An investigation of MAGIC vs. CHRISTINE runs indicated that about four to five harmonics are necessary for good accuracy. It is probable that only one or two harmonics of the sheath helix traveling wave are necessary, though; the requirement for four to five harmonics comes primarily from the space-charge model. Indeed, GATOR gave excellent agreement to MAGIC with only one harmonic of the sheath helix traveling wave. (GATOR used five space-charge harmonics, while MAGIC always includes all harmonics up to its time-step resolution, e.g., typically a hundred.) If harmonics are eliminated in either CHRISTINE or GATOR, the helix typically saturates at a power level 40–100% larger than realistic values. Hence, the use of modal methods, either GATOR or CHRISTINE, without harmonics turned on is extremely risky for design analysis. The obvious recommendation is therefore that any “default state” of these codes should have harmonics turned on.

The GATOR code presents an additional problem with regard to the harmonics. Apparently the GATOR code is based on *spatial* harmonics rather than temporal harmonics. This is in direct contrast to the physical picture of a temporally periodic signal. The simple mathematical property of being periodic leads to a Fourier series, e.g., temporal harmonics. Even in the PIC code which must necessarily contain startup harmonics, the picture is one of a periodic signal for a single input frequency. The spatial harmonics used in GATOR imply frequencies which deviate from harmonics of the input by the corresponding deviation of the dispersion relation from flatness. Obviously for a flat dispersion relation such as a vaned TWT, there is little difference between the temporal and spatial harmonics approaches. However, for unvaned helices and helices with strong tapers, the potential for discrepancy due to the use of spatial instead of temporal harmonics warrants some careful investigation. In fairness, and despite these reservations, it must be noted that GATOR has, in fact, been used to successfully model helix TWT's with very dramatic tapers for the Hughes Corporation.⁷

SECTION 3. BRILLOUIN B-FIELD COMPARISON

In this section, we investigate the importance of radial motion on the helix TWT performance. The basic picture is that, in real tubes, the beam typically expands as it slows down. The expanded beam lies on average closer to the helix, and therefore couples more strongly to it. The effect is sufficiently important that it should never be neglected in any design application. Since the 1-D modal method, CHRISTINE, cannot accommodate radial motion, it will not be discussed any further, except to point out that the most important area for improvement in the 1-D modal method would obviously be to add some type of radial expansion model.

3.1 IMPORTANCE OF RADIAL MOTION

Figure 3.1.1 shows a comparison of the previous infinite B-field drive curves to those at the Brillouin field for the 2-D PIC method. In the Brillouin field, the tube is seen to saturate at an input power which is 8 dB less than that required for saturation in the infinite field. In particular, whereas saturation was not seen at 7 cm in the infinite B-field case for input powers levels below 100 milliwatts, it is seen for a Brillouin field.

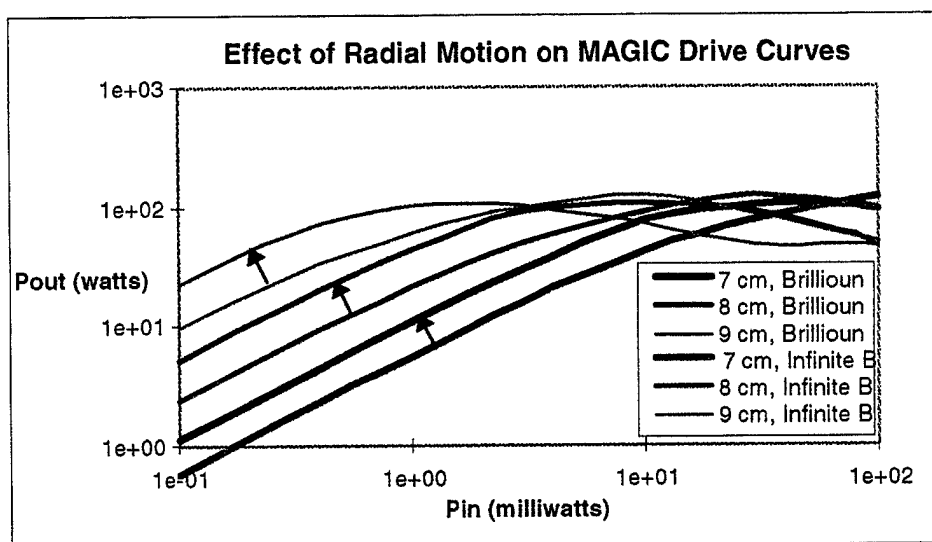


Figure 3.1.1 Comparison of infinite-B field and Brillouin B-field drive curves for the 2-D PIC method. The radial motion in the Brillouin field results in saturation 8 dB earlier, as indicated by the arrows, which is a very significant effect.

3.2 DRIVE CURVE

Figure 3.2.1 shows the drive curves at 7 cm for the Brillouin-focused TWT for the 2-D modal (GATOR) and 2-D PIC (MAGIC) methods. As before, there is excellent agreement in the linear growth regime, and in fact, all the way up to saturation. However, the post-saturation behavior is noticeably different. The 2-D PIC method (MAGIC) predicts a peak power at 7 cm of 112 watts when the input power is 40 milliwatts, while the 2-D modal method's peak is 115 watts and occurs at 30 milliwatts input. The 2-D PIC method (MAGIC) has a slower drop off in power after saturation than does the 2-D

modal method (GATOR), which explains the peak power condition at a slightly higher input power level. The power differences will be seen to correlate with subtle differences in the particle trajectory and phase-space plots in the following sections. An exact explanation for the differences is unknown, but the issue is explored further in the next section, including one possible conjecture. Drive curves at 8 cm and at 9 cm are not shown, but they further illustrate the differences between the methods in the post-saturation regime.

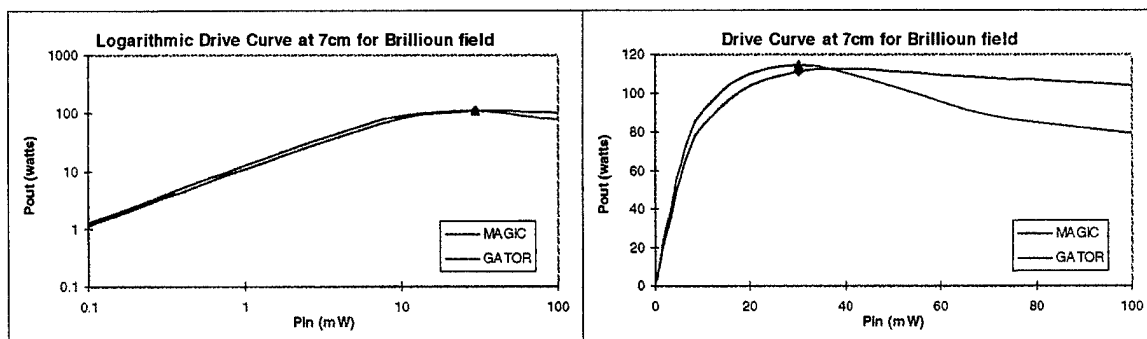


Figure 3.2.1 Brillouin field drive curve comparison at 7 cm. There is excellent agreement in the linear growth regime and up to saturation at 30 milliwatts. The behavior past saturation indicates significant differences between the methods. The exact reason for this difference is not known, but is investigated in the later sections.

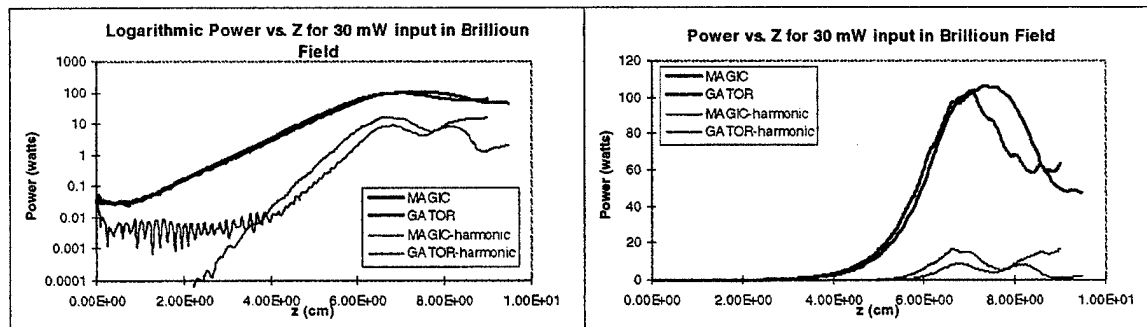


Figure 3.3.1 Growth of power in fundamental and harmonic vs. length down the tube for 30 milliwatts input power in a Brillouin focused TWT. There is excellent agreement up to saturation. Past saturation, the power drops off more rapidly in the 2-D modal (GATOR) method, but ultimately does not drop as low. (The apparent floor in PIC power is an artifact of a noise limitation on the power diagnostic.)

3.3 DETAILS OF SINGLE BRILLOUIN RUN

The markers at 30 milliwatts input power in the Figure 3.2.1 indicate the single run which will be examined in this section. Figure 3.3.1 shows the evolution of power in the fundamental and harmonic down the length of the TWT. The harmonic power shows the now familiar offset in magnitude and shift in the position of the dip that was seen in the infinite-B field scenario. The fundamental power shows truly remarkable agreement

up to saturation, on both the logarithmic and linear scale. Then, just as seen on the drive curves, there is significant departure past saturation.

Two features are worthy of comment. First is the more rapid drop in the power past saturation for the 2-D modal method. Second is that, despite the more rapid drop, the power ultimately does not fall as low as does the 2-D PIC method. The drop in power is due to the re-absorption of RF back onto the beam, caused by the slowed-down bunches having unfavorable phasing with regard to the RF. If space-charge forces were not present, the beam could re-accelerate and completely debunch, and the process would start over again. One possible explanation for the observed behavior in the 2-D modal method (GATOR) is that at saturation it is experiencing excessive space-charge forces. It is not possible to say conclusively that this is occurring, however, there is additional evidence supporting this conclusion.

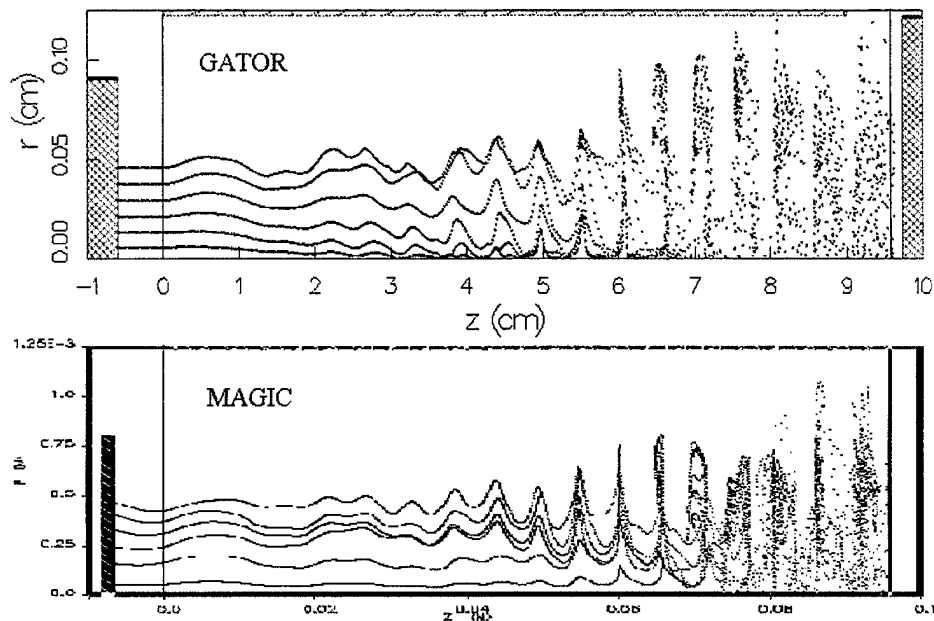


Figure 3.3.2 Particle trajectories for 30 milliwatts input into a uniform Brillouin magnetically focused helix TWT. The visible agreement in the radial motion between the 2-D PIC (MAGIC) result and 2-D modal (GATOR) result is pleasing. Identifiable differences include larger radial excursion of the GATOR beam and nonlaminarity of the outer part of the MAGIC beam.

Figure 3.3.2 shows the particle trajectories from the MAGIC and GATOR runs. The similarity between the 2-D PIC and 2-D modal results, especially in the radial motions of the particles in the Brillouin field, is quite pleasing. Care was taken to insure that both snapshots were taken at the same time during the RF cycle, and that six rays or emission points were used in both models. Are there any visible differences which might be linked to the discrepancy in the power past saturation? The 2-D modal (GATOR)

method shows slightly larger radial expansion. In addition, there is slightly more debunching near the end of the tube in the 2-D modal method (view the figure at an oblique angle to better discern this property). Both of these effects are consistent with excessive space-charge forces, resulting in more rapid debunching. The larger radial expansion is probably the cause of the more rapid decline in power, since the particles at higher radius couple more strongly to the wave, and hence reabsorb power more quickly after saturation. It is important to recall that for the infinite B-field case, there was only slight discrepancy in the power after saturation, so the larger discrepancy in the Brillouin case must almost necessarily be related to radial motion.

Additional visible differences between the two methods are the starting condition and laminarity of the beam at the input end. These issues are discussed in a later section involving PPM focusing, and are not thought to be greatly significant for the Brillouin case.

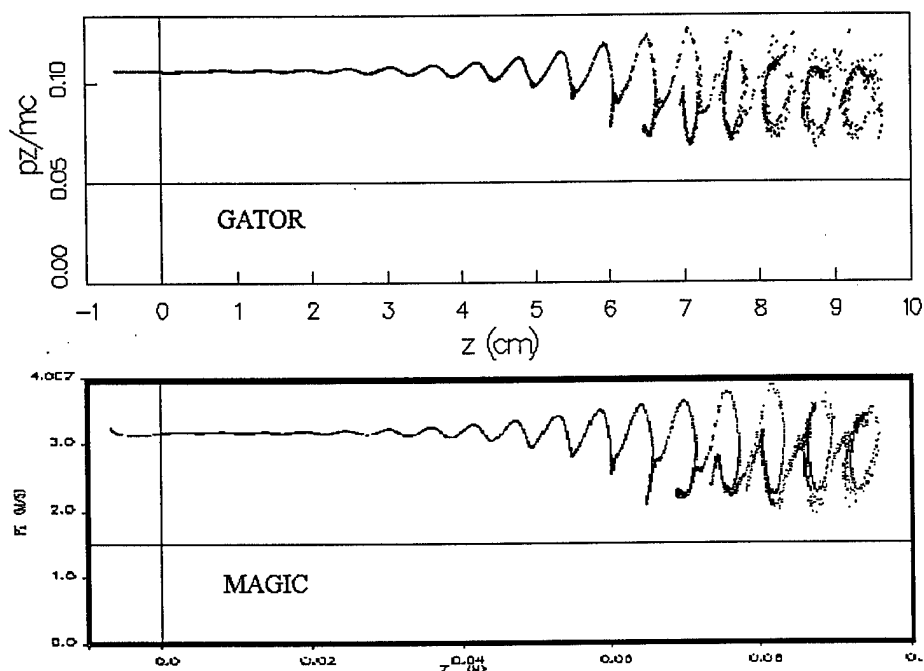


Figure 3.3.3 Particle phase-space for 30 milliwatts input into a uniform Brillouin magnetically focused helix TWT. The visible agreement between the 2-D PIC (MAGIC) result and 2-D modal (GATOR) result is notable. Identifiable differences include better preserved wave troughs and phase coherency past saturation in MAGIC.

Figure 3.3.3 shows the electron phase-space, which illustrates the differences between the two methods past saturation more clearly. Again, there is definitely greater debunching in the 2-D modal (GATOR) method, and in addition, the general outlines of the wave troughs appear to be less sharply defined than in the 2-D PIC method. Normally, such an effect is associated with numerical noise; however it seems counter-

intuitive to find a higher level of noise in the modal method than in the PIC method (PIC methods are famously noisy!). Perhaps in GATOR there is still some radius-dependent factor applied to each particle's space-charge force which should not be there, or some effect which remembers a particle's birth radius rather than using the actual radius of a particle. These suggestions are made because past saturation there is considerably more radial mixing, which would offer greater opportunity for noise generation from one of the aforementioned effects.

3.4 OUTLIER ELECTRON EFFECT IN GATOR

One impetus behind the study discussed in this paper was a fairly significant discrepancy between the body current originally predicted by the 2-D modal method, GATOR, and the 2-D PIC method. The modal method originally predicted greater than 10% of the beam striking the helix in a Brillouin field, while the PIC method indicated virtually no current to the helix. Experimental evidence eventually sided with the PIC method, and a search for a cause began. It was ultimately discovered that the outlier electrons in the modal method, those significantly beyond the mean radius, were experiencing unphysically large azimuthal velocities, consistent with an equilibrium at their large radius, rather than the initial equilibrium at a much smaller radius. This defect in the model was remedied, and the result was dramatically improved beam confinement, such that virtually no current to the helix occurred, in accordance with the experimental observations. From a practical point of view, the identification and remedy of this previous adverse effect in the 2-D modal method is probably the most important achievement of the work discussed here. All results presented in this and the following sections include the proper treatment of the outlier electrons.

3.5 EMISSION CONDITION AND NONLAMINAR FLOW IN MAGIC

Laminar flow of a beam in a uniform magnetic field is possible. The electrons must have an azimuthal velocity such that the $v_\theta \times B_z$ force exactly cancels the E_r space-charge force. For the nonrelativistic flat current profiles used in this study, the angular velocity is a function of radius:

$$v_\theta(r) = \frac{1}{2} r \left[\Omega_c - \sqrt{\Omega_c^2 - 2\omega_p^2} \right],$$

where $\Omega_c = eB_{z0}/m_e$ is the electron cyclotron velocity, and $\omega_p = (ne^2/\epsilon_0 m_e)^{1/2}$ is the plasma frequency of the beam. The Brillouin field condition, $\Omega_c = \sqrt{2} \omega_p$, is obvious, and at exactly the Brillouin field $v_\theta(r) = \frac{1}{\sqrt{2}} \omega_p r$.

There is a noticeable nonlaminarity of the MAGIC beam lines early on. It was eventually discovered that this was due to a peculiar effect of the finite-difference force algorithm within the MAGIC code. The particles feel a force which is partially averaged, and then linearly interpolated, over its nearest two radial cells. The result is an artificial rounding of the sharp corner in the force profile. The same result would occur if the edge of the beam profile were slightly smoothed, instead of making a perfect step function. An illustration is shown in Figure 3.3.2. In later runs, it was found possible to partially remedy this effect by giving the outer electrons in MAGIC a smaller amount of azimuthal

velocity, consistent with the reduced forces that were felt. However, perfect laminar flow remained difficult, and clearly it would be beneficial for the MAGIC code to have this effect treated internally in a self-consistent manner, e.g., as a Brillouin emission option.

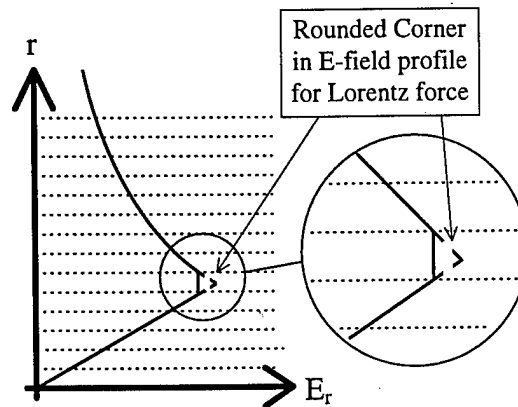


Figure 3.5.1 Illustration of the cause behind the non-laminar flow in the outer electrons of the 2-D PIC beam trajectories. The force profile is artificially rounded, resulting in a force which is smaller than analytically calculated.

Another apparent difference, also due to a peculiarity of the 2-D PIC method, is the starting condition at the metal surface. It will be noted, that both methods start the beam about 7 mm before the zero coordinate, where the RF enters. The 2-D PIC method can only emit particles from a conductor surface. Once emitted, at the full 3.0 kVolt beam energy, the electrons experience a space-charge depression, which slows them down by about 12 volts. In 2-D PIC, this is an entirely natural result of having the parallel, e.g., radial, electric field be zero on the metal surface and become non-zero a short distance away, due to the DC space-charge of the beam. Unfortunately, the axial reduction in velocity must also be accompanied by a slight radial impulse, which causes an undesirable initial scalloping of the beam in the 2-D PIC model. In the 2-D modal method, the initial space-charge depression is computed analytically and is applied to the beam energy before emission. In addition, there is no requirement for a boundary condition on the electrostatic field at the emission surface. Hence, beam creation in the 2-D modal method can be made absolutely laminar, as evidenced by the perfect flat trajectories before the RF region.

3.6 RADIAL SHEAR

Radial shear occurs when electrons in the outer part of the beam experience slightly different axial accelerations than electrons in the inner part of the beam. There can be DC sources of radial shear and AC sources of radial shear. The DC sources of radial shear arise within the diode region and where the magnetic field immersion of the beam is changing. DC sources of radial shear inevitably result in the outer part of the beam going slightly slower than the inner. The AC source of radial shear is due to the radial profile of the RF axial field inside of the helix, with particles closer to the helix receiving a slightly larger axial force than particles on axis.

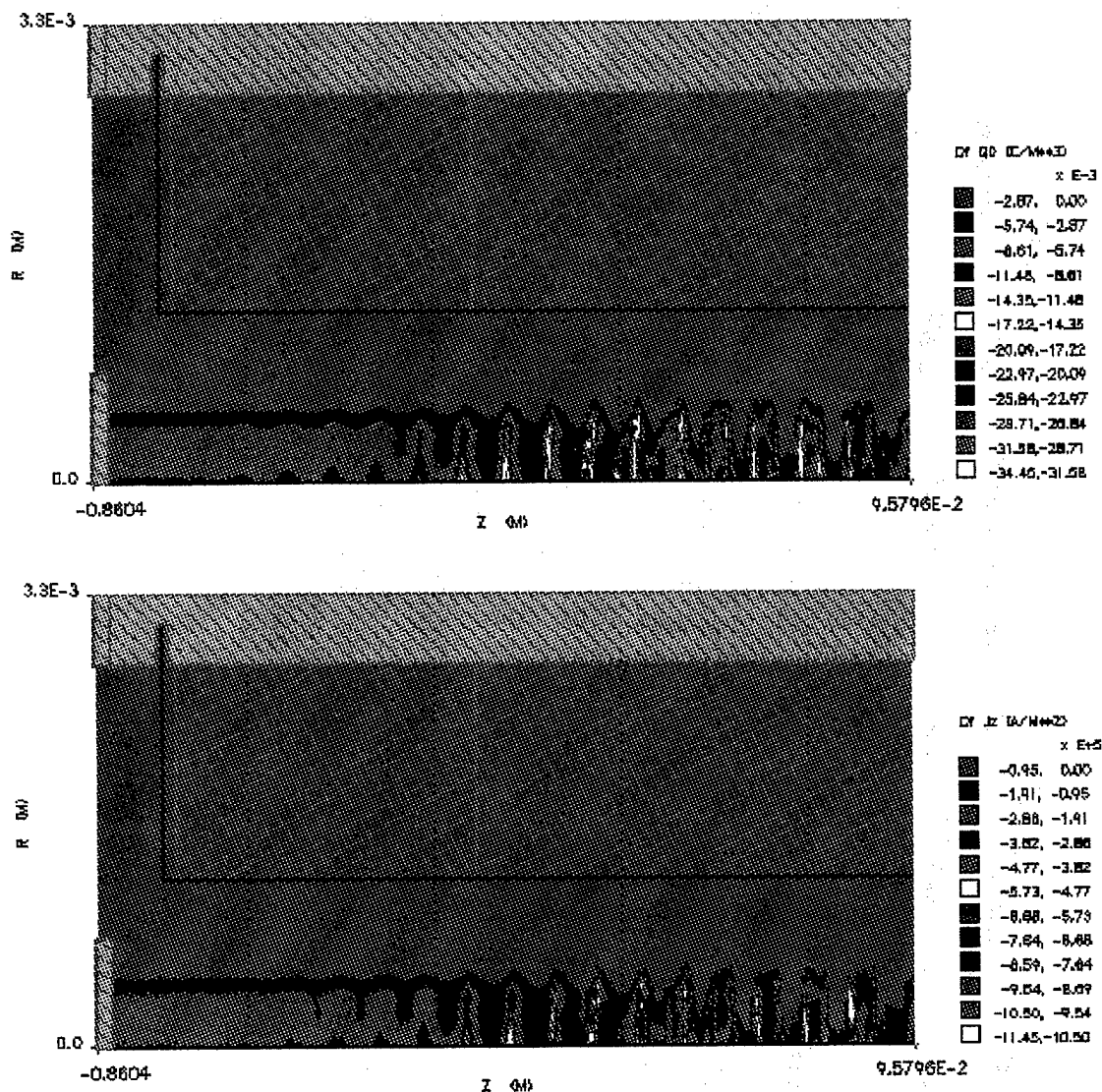


Figure 3.6.1 Contours of charge (top) and axial current (bottom). Radial shear is evident before saturation and appears to reverse after saturation; however, the direction of tilt is counter-intuitive, since outer electrons are expected to slow more than inner electrons prior to saturation.

Figure 3.6.1 shows contours of space-charge and contours of axial current, e.g., charge times velocity, from the 2-D PIC method (MAGIC). Both figures contain similar patterns, indicating that radial shear in the velocity is imperceptible compared to space-charge separation as far as current bunching is concerned. Hence, the only indication of radial shear is the accumulated effect which it has on the space-charge separation. It appears as if there is some evidence of radial shear, with a noticeable tilt of the bunch towards the output end of the TWT before saturation, and possibly a reversal of this slope after saturation.

This result seems to be counter-intuitive, since the outermost electrons should experience stronger deceleration than the inner electrons, by virtue of their proximity to

the helix, and hence the bunch should tilt towards the input end of the TWT. No explanation for this counter-intuitive observation on the shear is offered here.

SECTION 4. PPM B-FIELD COMPARISON

Additional simulations were performed with the 2-D modal (GATOR) and 2-D PIC (MAGIC) methods replacing the uniform Brillouin field with a PPM field. The exact formula used for the PPM field in both methods was:

$$B_z(z,r) = B_{z0} I_0(k_{ppm} r) \sin(k_{ppm} (z-z_0)),$$

$$B_r(z,r) = -B_{z0} I_1(k_{ppm} r) \cos(k_{ppm} (z-z_0)),$$

where the peak field on axis was $B_{z0} = 1.326$ kGauss ($= 1.414 \times$ Brillouin field), the PPM length was 0.6604 cm, e.g., $k_{ppm} = \pi/0.6604 \text{ cm} = 4.757 \text{ cm}^{-1}$, and the axial position of the PPM's was selected so that there was a B_z null exactly at the emission point, 0.2 cm before the location where RF was introduced, e.g., $z_0 = -0.1302$ cm. The angular velocity given to the beam at the emission point was the same as for the Brillouin field, e.g., $v_\theta(r) = \frac{1}{\sqrt{2}} \omega_p r$.

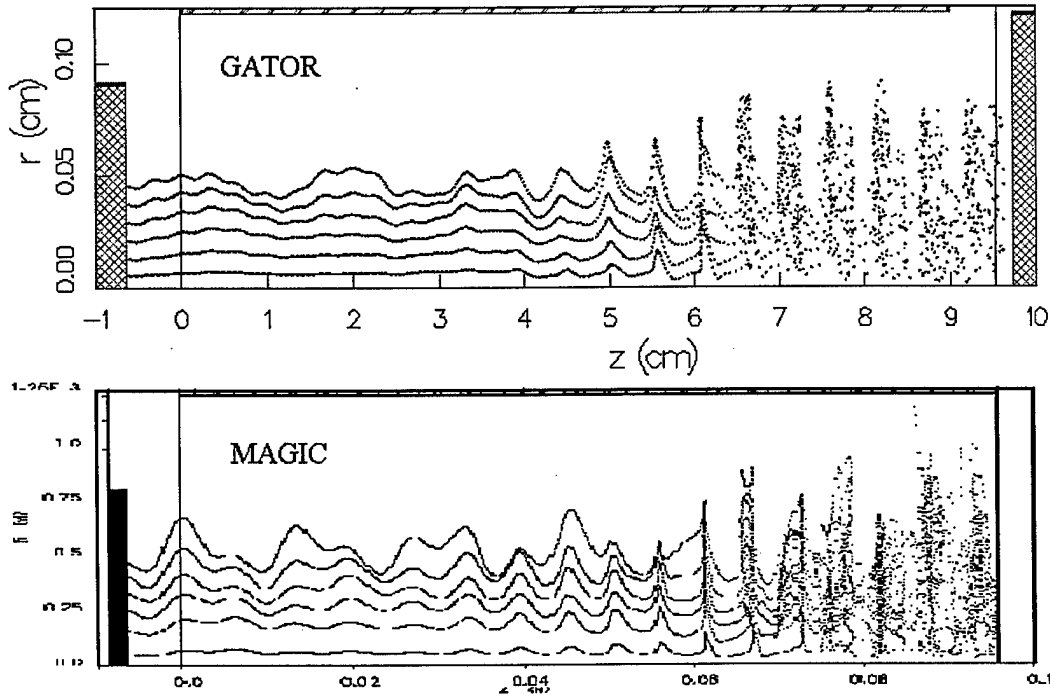


Figure 4.1 Particle trajectories for 30 milliwatts input into a PPM focused helix TWT. The axial bunching is in good agreement, but the differences in radial motion in the PPM field distract from a good comparison. The MAGIC code suffers significantly from emission mismatch difficulties and a force smoothing effect on the outermost ray.

Figure 4.1 shows the particle trajectories for 30 milliwatt input power into a PPM focused tube. The axial bunching is in good agreement, as was the case with the Brillouin field. However, the radial motion is visibly quite different between the two cases. In particular, the 2-D PIC method (MAGIC) suffers from significant mismatch at the emission point, which leads to much greater scalloping than for the 2-D modal (GATOR) method. As previously discussed, the 2-D PIC method must emit particles from a conducting metal boundary which suppresses the radial electric field, and causes a local mismatch. Attempts to compensate for the mismatch by altering the radial velocity at emission were largely unsuccessful. This remains a difficult problem for the 2-D PIC method. An alternative to launching from a metal is to import a beam and its associated electric field from a previous run. This previous run would, of course, have to be a gun-type run, which would require proper design of the gun so that a good focus was achieved, a possibly time-consuming task. An alternative would be, in the future, to endow the PIC code, MAGIC, with an ideal Brillouin beam emission capability, which would, in principle, generate the import beam and field internally to satisfy the ideal Brillouin flow condition, or the ideal PPM confinement condition.

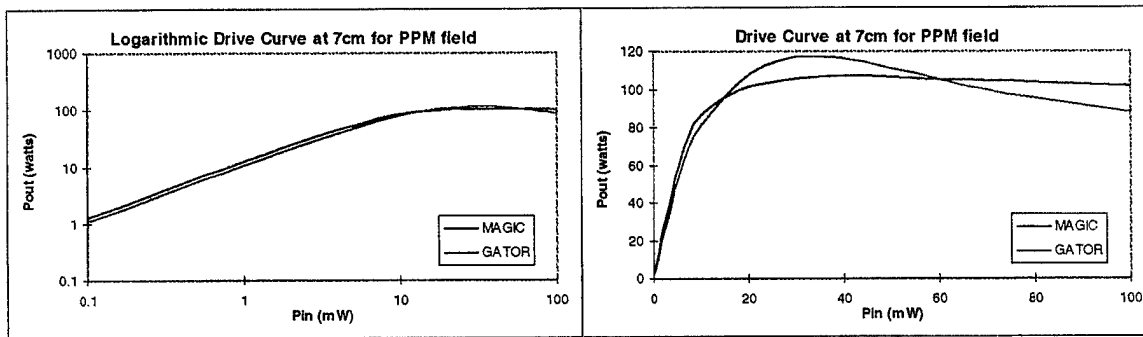


Figure 4.2 PPM field drive curve comparison at 7 cm. There is excellent agreement in the linear growth regime, but divergence at saturation which occurs at 30 milliwatts. The disagreement past saturation is similar to that observed for the Brillouin field.

It is also interesting to note that the 2-D modal (GATOR) beam confinement after saturation is improved over that from the Brillouin field run, and is equal to that from the 2-D PIC (MAGIC) method. In the previous section it was hypothesized that the particles in GATOR were experiencing excessive space-charge forces after saturation, which caused the poorer beam confinement. These same forces should be at work in the PPM case; however, somehow, they do not result in loss of beam confinement, possibly as a result of the oscillatory nature of the static fields seen by the particle.

Figure 4.2 shows the drive curves at 7 cm for the PPM focusing field. The overall trends are similar to the Brillouin case, with good agreement in the linear regime, and a noticeable divergence after saturation. In fact, the divergence occurs earlier, slightly before saturation for the PPM case, probably a result of the additional scalloping in the 2-D PIC method (MAGIC). The behavior past saturation shows the more rapid drop in power for the 2-D modal (GATOR) method, similar to the Brillouin case, indicating that whatever was causing this effect in the Brillouin field is probably also at work in the PPM run.

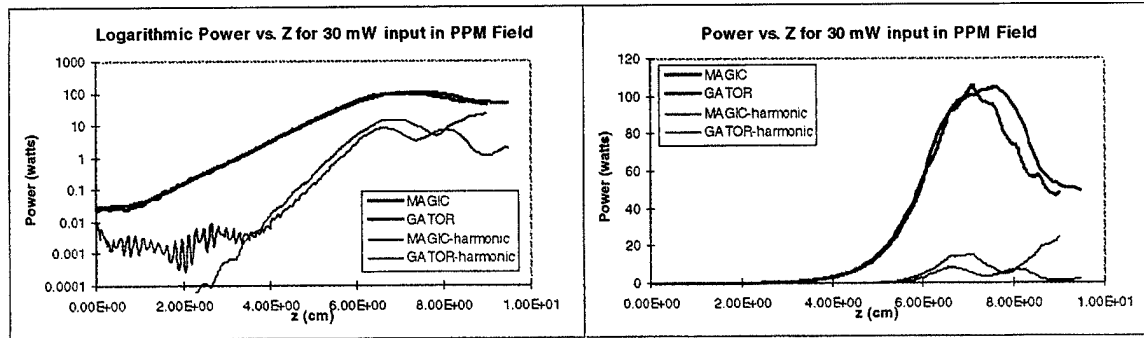


Figure 4.3 Growth of power in fundamental and harmonic vs. length down the tube for 30 milliwatts input power in a PPM focused TWT. There is excellent agreement up to saturation. Past saturation, the power drops off more rapidly in the 2-D modal (GATOR) method, but is still in better agreement than with the Brillouin case.

Figure 4.3 shows the growth in power down the tube for the 30 milliwatt input power case. The figure shows all of the previously established features, e.g., good agreement in the linear regime, faster drop in power for the 2-D modal method after saturation, and marked differences in the harmonic after saturation. Nevertheless, the agreement after saturation is better than in the Brillouin case. Given that the 2-D modal method's radial confinement is better for PPM confinement, it is likely that the hypothesized excessive space-charge forces are strongly correlated with radial expansion of the beam.

Figure 4.4, showing the particle phase-space for the 30 milliwatt case corroborates this hypothesis. The agreement between the methods after saturation is visibly better than for the Brillouin case. In particular, the 2-D modal method's bunches are not as spread out, and are less noisy. Thus, despite the obvious mismatch in the beam trajectories, the better radial confinement results in a closer match in the phase-space past saturation.

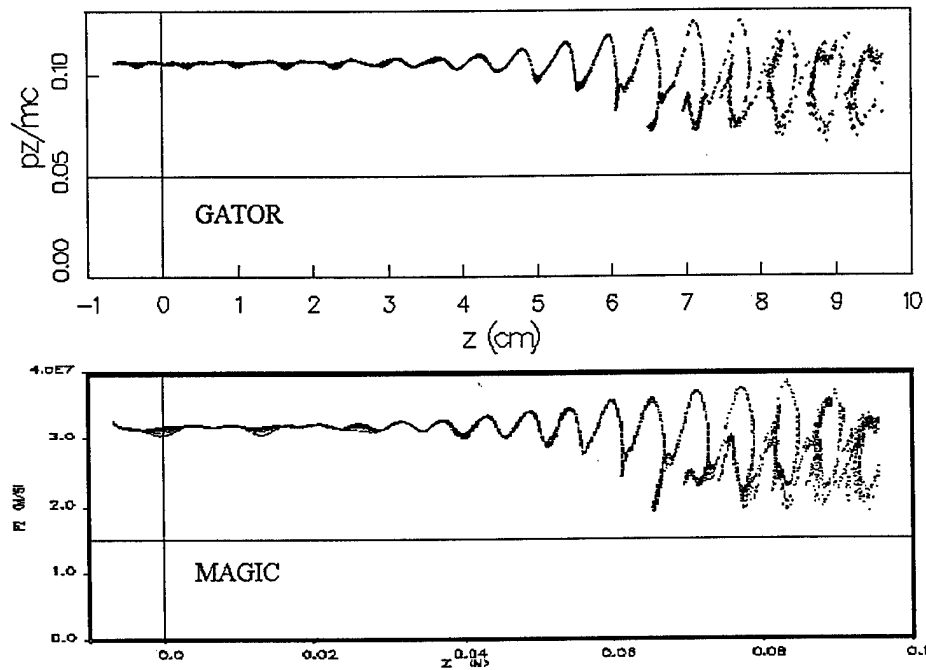


Figure 4.4 Particle phase-space for 30 milliwatts input into a PPM focused helix TWT. The visible agreement between the 2-D PIC (MAGIC) result and 2-D modal (GATOR) result is better than for the Brillouin focused beam, probably because of better radial confinement.

SECTION 5. ANALYSIS OF ACCURACY

Most of this section will discuss accuracy of the modal methods, since these methods are simplifications of the Maxwell field equations, whereas the PIC method does not simplify these equations. The PIC method does involve a simplification, though, namely the course-graining of space, and this aspect will also be discussed. (All three methods simplify by ignoring the third dimension.)

One of the most difficult and sometimes frustrating aspects of working with design codes is the inherent uncertainty as to their accuracy in some new regime being explored. Most design codes are based on a set of assumptions which have validity criterion which are easily expressed in a mathematical form, and which are readily calculable from information within the design code itself; yet very few bother to evaluate the validity criterion. The omission is time saved by the code programmer who might be under a tight deadline, but the cost in time for the user can be enormous. Whenever possible, mathematical validity criterion should be evaluated and displayed, in order to help the user judge accuracy in a new parameter regime, instead of relying on anecdotal advice.

5.1 ELECTROMAGNETIC / ELECTROSTATIC SEPARATION

The analysis of the 2-D modal method, GATOR, involves the independent computation of the wave electric field and an electrostatic field, e.g., the electric field is the sum of two different electric fields, each of which obeys a different evolution equation. (In GATOR, the electrostatic field is further divided into AC and DC space-charge parts.) The electromagnetic / electrostatic division is a fairly common practice in a wide variety of plasma physics problems, when either a propagating electromagnetic wave is mildly affected by space-charge, or when a propagating electromagnetic wave interacts with a space-charge wave in a small, spatially-localized region. (The CHRISTINE code is actually based on a single electric field model, and thus does not pertain to the discussion in this section.)

The separation of the electric field into two distinct parts naturally leads one to the vector-scalar potential formalism, since this formalism similarly desires to separate Maxwell's equations into electromagnetic and electrostatic parts. The monopole equation, $\nabla \cdot \mathbf{B} = 0$, establishes the existence of a vector potential, \mathbf{A} , such that $\mathbf{B} = \nabla \times \mathbf{A}$. Faraday's Law, $\partial_t \mathbf{B} + \nabla \times \mathbf{E} = 0$, establishes the connection between the electric field and the vector potential, $\partial_t \mathbf{A} + \mathbf{E} + \nabla \phi = 0$, with ϕ , the scalar potential, being a completely arbitrary scalar function, similar to a constant of integration. The specification for the arbitrary scalar field, ϕ , is called the gauge. The obvious reason for having a non-zero scalar potential becomes apparent when one takes the Fourier transform ($\partial_t \Rightarrow -i\omega$) of the Faraday Law relationship, rearranged here with just \mathbf{E} on the left hand side:

$$\mathbf{E}_\omega = i\omega \mathbf{A}_\omega - \nabla \phi_\omega .$$

Since $\mathbf{E}_\omega(\omega=0)$ may be non-zero, it implies either that $\mathbf{A}_\omega(\omega=0)$ must go to infinity (an undesirable property), or that $\nabla \phi_\omega(\omega=0)$ is non-zero (a much better alternative). Thus,

whatever gauge is selected, clearly it is desirable that $\mathbf{E}_\omega(\omega=0)=-\nabla\phi_\omega(\omega=0)$. Ampere's Law and Gauss's Law give the evolution equations for the two potentials,

$$\omega^2 \mathbf{A} - c^2 \nabla \times \nabla \times \mathbf{A} + i\omega \nabla \phi + \mathbf{J}/\epsilon = 0 \quad ,$$

$$\nabla^2 \phi - i\omega \nabla \cdot \mathbf{A} + \rho/\epsilon = 0 \quad ,$$

where the “ ω ” subscript has been dropped. The specification of a particular gauge is often used to simplify the above equations even further, but is not necessary for our purposes.

A Poynting theorem for the potentials can be created by multiplying the complex conjugate of the vector equation by $i\omega\epsilon\mathbf{A}$, multiplying the scalar equation by $i\omega\epsilon\phi^*$, with the substitution, $\rho=\nabla\cdot\mathbf{J}/(i\omega)$ from the charge continuity equation, and adding together the two equations. The result is:

$$\begin{aligned} & \nabla \cdot \left[\frac{i\omega}{\mu} \mathbf{A} \times \nabla \times \mathbf{A}^* \right] + \nabla \cdot \left[\phi^* (\mathbf{J} - i\omega\epsilon(i\omega\mathbf{A} - \nabla\phi)) \right] + \\ & i\omega\epsilon|\omega\mathbf{A}|^2 - \frac{i\omega}{\mu} |\nabla \times \mathbf{A}|^2 - i\omega\epsilon |\nabla\phi|^2 + \\ & i\omega\mathbf{A} \cdot \mathbf{J}^* - (\nabla\phi^*) \cdot \mathbf{J} = 0 \end{aligned}$$

The first term is recognizable as the “electromagnetic” part of the $\nabla \cdot (\mathbf{E} \times \mathbf{B})$ Poynting flux. The second term is a new quantity, which is sometimes referred to as the “kinetic” flux. It is proportional to electrostatic potential. Note that at zero frequency, the electromagnetic Poynting flux is zero, and the kinetic flux is just $\phi^* \mathbf{J}$, e.g., the electrostatic potential energy carried by the particle motion. The second line of the energy balance equation consists of purely imaginary terms representing the field energy, and the last line of the energy balance equation is the $\mathbf{E} \cdot \mathbf{J}$ work term, with a real part that matches $\mathbf{E} \cdot \mathbf{J}^*$, but a different imaginary part.

There are, of course, an infinite variety of ways to combine the two potential equations into Poynting-like energy balance equations. However, if the “electromagnetic” part of the Poynting flux is to be isolated from the zero-frequency $\mathbf{E} \times \mathbf{B}$ energy, as desired, it is obviously necessary to introduce a secondary “kinetic” flux similar to that illustrated. The kinetic flux at non-zero frequencies often plays an important phenomenological role; in the case of GATOR, it appears as the “AC space-charge.” The important point to note is that the kinetic flux at non-zero frequencies depends on the choice of gauge, e.g., on the choice of the integration constant ϕ . The kinetic flux itself can be rewritten as

$$T_{kinetic} = \phi^* (\mathbf{J} - i\omega\epsilon(i\omega\mathbf{A} - \nabla\phi)) = \phi^* \nabla \times \nabla \times \mathbf{A} \quad ,$$

which illustrates that it is intrinsically a cross-term between vector and scalar potentials. There is a direct, but seldom realized, connection between a phenomenologically derived form of the kinetic flux and the gauge. It is not possible to derive a kinetic flux and choose a gauge, e.g., the Coulomb gauge, independently. Attempts to do so very often result in null- or double-counting of terms in the power balance.⁸ In the 2-D model, GATOR, the coulomb gauge is used as a basis of the AC space-charge field. It is not known whether the AC space-charge power, e.g., the kinetic flux, is computed.

5.2 MODAL METHOD BASED ON POTENTIALS

In a cold test of an attenuation and reflection-free TWT, $\phi=0$, and there is a vector potential, \mathbf{A}_0 , which satisfies $\nabla \cdot \mathbf{A}_0=0$ and $c^2 \nabla^2 \mathbf{A}_0 + \omega^2 \mathbf{A}_0=0$, and which we shall normalize such that the Poynting flux is unity:

$$\text{Re} \left\{ \hat{\mathbf{z}} \cdot \frac{1}{\mu} (\mathbf{E}_0 \times \mathbf{B}_0^*) \right\} = \text{Re} \left\{ \hat{\mathbf{z}} \cdot \frac{i\omega}{\mu} (\mathbf{A}_0 \times \nabla \times \mathbf{A}_0^*) \right\} = \text{Re} \left\{ \frac{i\omega}{\mu} (\mathbf{A}_0 \cdot \partial_z \mathbf{A}_0^* - \mathbf{A}_0 \cdot \nabla \mathbf{A}_{0z}^*) \right\} = 1 .$$

Given that there is no attenuation and no reflection, the above should be true all along the z-direction. The cold-test vector potential, \mathbf{A}_0 , is the TWT "mode," and the "modal" method is derived by assuming that in the general case, the vector potential is given by:

$$\mathbf{A} \equiv a(z) \mathbf{A}_0 .$$

In other words the vector potential is the product of the cold-test vector potential and an amplitude function, $a(z)$, of just the tube axis direction, z . With the unit normalization of the cold-test vector potential, it follows that the Poynting flux associated with the vector potential is just $P = a^2(z)$. Under the modal assumption, the electric and magnetic fields are given by:

$$\mathbf{E} = i\omega a \mathbf{A}_0 - \nabla \phi ,$$

$$\mathbf{B} = a \nabla \times \mathbf{A}_0 + a' \mathbf{z} \times \mathbf{A}_{0\perp} ,$$

where a' designates $\partial a / \partial z$. It is important to note that the modal assumption is not a choice of gauge; it is an assumption on the character of the transverse electric field. As such, it represents an approximation, which should be verified to insure that it remains valid. The best way to verify the approximation is simply to insert the approximate fields into Gauss's and Ampere's Law and examine the error.

It is convenient to separate out from the potential, ϕ , a part which is proportional to the mode growth, a' ,

$$\phi = \Phi + i \frac{c^2}{\omega} a' A_{0z} ,$$

with the remaining potential denoted as Φ . When the fields are plugged into Gauss's Law, the result is:

$$\nabla^2 \left(\Phi + i \frac{c^2}{\omega} a' A_{0z} \right) = \frac{-1}{\epsilon} \rho + i \omega a' A_{0z} \quad .$$

When the above fields are plugged into the complex conjugate of Ampere's Law and then dotted with $i\omega\epsilon A_0/2$, the result is:

$$\frac{i\omega}{\mu} (\mathbf{A}_0 \cdot \partial_z \mathbf{A}_0^* - \mathbf{A}_0 \cdot \nabla A_{0z}) a' = -\frac{i\omega}{2} \mathbf{A}_0 \cdot (\mathbf{J}^* - i\omega\epsilon \nabla \Phi^*) + \frac{i\omega}{2\mu} (|A_{0z}|^2 - |\mathbf{A}_{0\perp}|^2) a'' \quad .$$

Note that the term in from of a' is just the z-directed Poynting flux of the cold-test mode, which was normalized to unity. Assuming that a is pure real, take the real part of the above equation to get the evolution equation for the mode amplitude, a :

$$a' = -\text{Re} \left\{ \frac{i\omega}{2} \mathbf{A}_0 \cdot (\mathbf{J}^* - i\omega\epsilon \nabla \Phi^*) \right\} \quad .$$

This equation is essentially the electromagnetic $\mathbf{E} \cdot \mathbf{J}$ with the usual additional space-charge correction term. Note that the previous equation for the space-charge correction term, Φ , contains terms in a' , the growth rate, which are usually ignored, in order to prevent the two equations for a' and Φ from being coupled. These terms are $i\omega\epsilon a' A_{0z}$ compared to the charge, ρ , and $i(c^2/\omega)a' A_{0z}$ compared to the potential Φ . Obviously, a good test of the validity of the space-charge model in GATOR would be to compare the magnitudes of these terms.

5.3 ACCURACY CHECK FOR THE MODAL METHODS

The analysis for the 1-D modal method, CHRISTINE, is not based on a separation of power into electromagnetic and electrostatic parts. Rather, it is based upon the following equation for electric field, which is exact:

$$\left[\nabla^2 + \frac{\omega^2}{c^2} \right] \mathbf{E} = -i\omega\mu_0 \left[1 + \frac{c^2}{\omega^2} \nabla \nabla \right] \cdot \mathbf{J} \quad .$$

When there is no radial motion, the $\nabla_{\perp} \cdot \mathbf{J}_{\perp}$ terms vanish, resulting in considerable simplification. The "forward propagating mode" assumption then results in the substitution:

$$\partial_z \rightarrow -i \frac{\omega}{v_{ph}} \quad ,$$

where v_{ph} is the circuit phase velocity. Only radial derivatives remain, which form a fairly typical radial boundary value problem, with the usual Bessel function solutions. So where was the approximation? It was, in fact, essentially, the same as the neglect of the amplitude growth rate terms, a' , from the previous analysis. A more accurate modal approximation would use the following substitution:

$$\partial_z \rightarrow -i \frac{\omega}{v_{ph}} + \frac{a'}{a} ,$$

since the axial derivative involves both the wave variation and the amplitude variation. Normally the amplitude variation is negligible, but for large mode amplitudes, they can start to approach the axial current terms in magnitude. In particular, if we look at the neglect of the $i\omega\epsilon a' A_{0z}$ term with respect to ρ in the analysis of the previous section, which is more suitable to the GATOR approach, this requires that:

$$\frac{a'}{a} \ll \frac{J_z}{v_{ph} \epsilon E_z} ,$$

in addition to the obvious requirement for any modal method that

$$\frac{a'}{a} \ll \frac{\omega}{v_{ph}} .$$

It can be seen that as E_z increases, while a'/a and J_z stay roughly the same, the restriction becomes more difficult to satisfy. In addition, the occurrence of a zero amplitude, $a \approx 0$, as often occurs for the harmonic after saturation, is a clear violation of these approximations. It would be prudent for all modal methods to evaluate the above conditions to indicate to the user where there might be known violation of the physical approximations.

In the case of the 2-D modal method (GATOR), it also seems obvious that the code should evaluate the error in Gauss's Law, $\nabla \cdot \mathbf{E} - \rho/\epsilon$, since some aspects of the space-charge model may be in question. This is admittedly a difficult task for the programmer, since \mathbf{E} is a complicated summation of different terms. Nevertheless, it would be of tremendous benefit for the user, and might point the way towards future improvements to the model.

The modal codes should also perform particle-plus-field energy balances if they do not already. No energy balance mismatches were observed in the course of this study, nevertheless, energy imbalance is often the first sign of poor grid resolution, which an inexperienced user might unknowingly encounter. Also, repeating a conclusion of Section 3.2, it is not known whether there is net power associated with the AC-space-charge forces in GATOR, and whether or not it should be included in the power balance.

5.4 ACCURACY CHECK FOR THE PIC METHOD

The accuracy of the Finite-Difference Particle-in-Cell (FD-PIC) method is primarily dependent on sufficient resolution of the physics of interest in terms of sufficiently small space and temporal grids and a sufficiently large number of particles. The accuracy is, therefore, typically tested by doubling the number of cells and/or particles, and verifying that the answer does not change significantly.

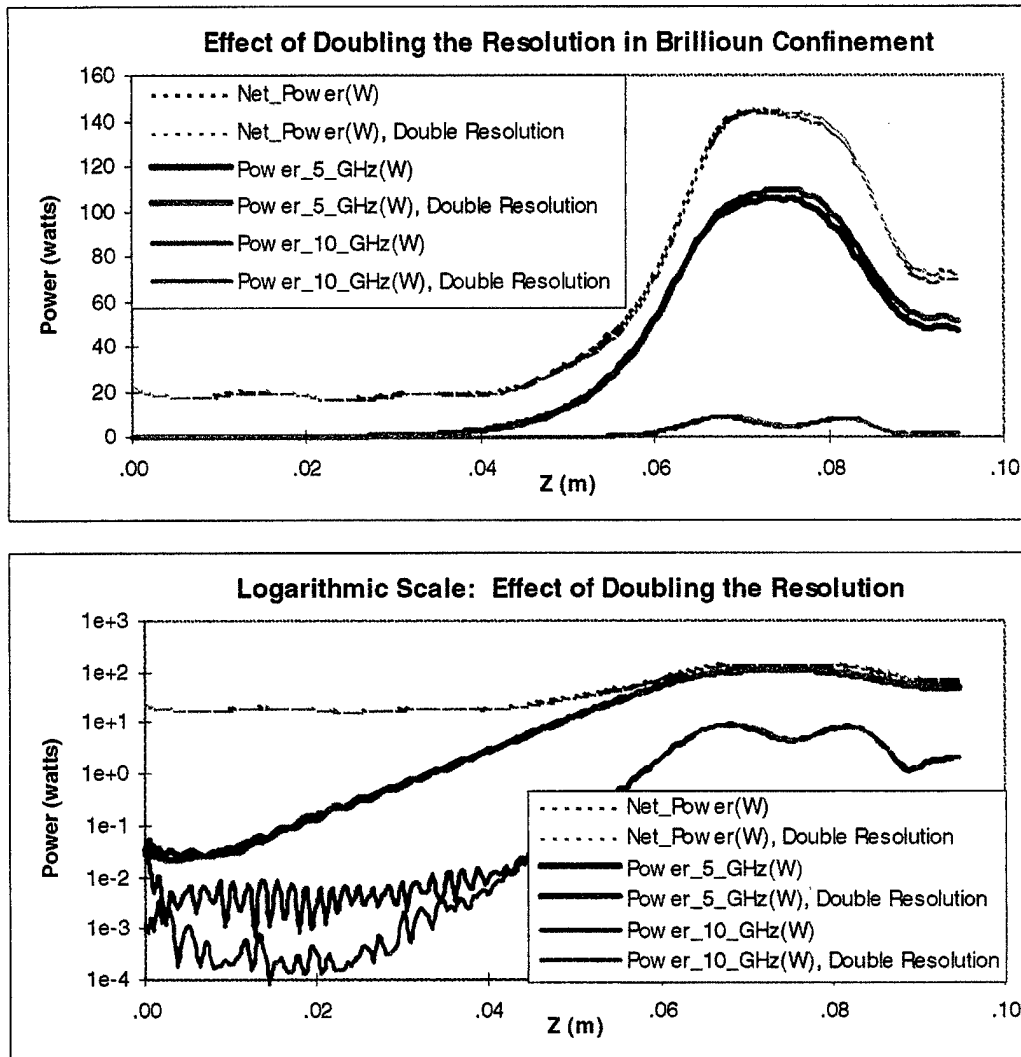


Figure 3.4.1 Accuracy check for the 2-D PIC method (MAGIC), by doubling the number of radial cells and the number of particles. The saturated power increased slightly from 105.8 to 109.5 watts. All physical behavior remained identical, including no apparent change to the harmonic. The artificial floor on the power diagnostic was lowered for unknown reasons.

The run using PPM confinement at 30 milliwatts input power was rerun, with twice the resolution in terms of the radial grid, time step, and number of particles. The results are shown in Figure 3.4.1. The run time increased by a factor of 5. The results are summarized in the Figure below. Most significant was a slight increase in the saturated

power from 105.8 to 109.5 watts, a 3.5% change. The power difference remained at the same level for positions beyond saturation. The position of saturation changed by half an axial grid cell. Also, an unexpected lowering of the Poynting Splitter diagnostic's floor occurred, which remains unexplained.

SECTION 6. SUMMARY

The basic conclusion of this comparison is that the codes are in excellent agreement up to saturation. Given that practical TWT's are rarely, if ever, built to operate beyond saturation, it is safe to say that all methods are recommended for design of practical TWT's.

The one important physical difference between the methods is the lack of radial expansion in the 1-D modal method (CHRISTINE). This is an important effect, which prevents CHRISTINE from being confidently used for high-accuracy design work, unless the design has very strong and effective beam confinement. It may be possible to endow CHRISTINE with a radial expansion model in the future, and this would surely be a very worthwhile endeavor.

Despite boasting the most self-consistent treatment of the three methods for high-accuracy design work, the 2-D PIC method suffers from several aspects which make its application to TWT design difficult for non-experts. Run times are small enough that a single TWT can be run in about 2 hours. This is good for cross-checking a design point, or perhaps evaluating a single parameteric variation, but is not useful for exploration of large regions of parameter space. Several other peculiarities of the PIC method are also nuisance factors, such as the difficulty with the low-level noise in the power diagnostic, and the beam launching mismatch difficulty.

The 2-D modal method (GATOR) lies between the extremes of the 1-D modal (CHRISTINE) and 2-D PIC (MAGIC) methods, and clearly this approach is situated to be a workhorse design tool. Run times are sufficiently fast enough to explore large regions of parameter space, and the inclusion of radial motion makes this method suitable for high-accuracy design work. The primary challenge facing the 2-D modal method is to adequately predict not only the TWT performance, but to also predict the limitations of its space-charge model, without requiring the user to become engaged in a lengthy period of investigation. Careful analysis of the approximations involved in the method are also likely to result in improvements to the space-charge model, although it is unlikely that an "optimum" space-charge model exists.

In the rare event where accurate analysis beyond saturation is required, this study indicates that the 2-D modal method's space-charge model is probably inadequate, and hence 2-D PIC should always be used, at least until improvements are made to the other methods.

Some behaviors observed in this study remain "mysterious" and warrant further investigation. The most important is probably the difference in the behavior of the harmonics near saturation. Here both modal methods agree, but disagree with the PIC method. Also, the counter-intuitive slope of the radial shear remains unexplained.

REFERENCES

- ¹ B. Goplen, L. Ludeking, D. Smithe, and G. Warren, *Computer Physics Communications* **87** (1&2), May 1995.
- ² H. P. Freund and E. G. Zaidman, *Physics of Plasmas* **4** (6), June 1997.
- ³ Unpublished results, experimental data from Northrop Grumman Corporation, ref. David Whaley.
- ⁴ T. Antonsen, Jr. and B. Levush, NRL/FR/6840-97-9845, May 1997.
- ⁵ D. Whaley, C. Armstrong, B. Gannon, G. Groshart, E. Hurt, J. Hutchins, M. Roscoe, T. Antonsen, and B. Levush, *IEEE Transactions on Plasma Science* **26** (3), June 1998.
- ⁶ David Whaley, private communication.
- ⁷ Henry Freund, private communication.
- ⁸ Y. Y. Lau, D. Chernin, *Physics of Fluids B* **4** (11), November 1992.

To: Ms. Mary Templeman
By: Mary Anne Kodis
Date: 15 July 1998
Subject: Annual Report, Contract 96-C-2047

Ms. Templeman:

Please assign a Distribution Statement A (Unlimited Distribution) to the document "Comparison of Helix TWT Simulation Using 2-D PIC (MAGIC), 2-D Modal (GATOR), and 1-D Modal (CHRISTINE) Methods." This is the final report of the base year of contract N00014-96-C-2047.

Thank you.

Mary Anne Kodis

Mary Anne Kodis
CCR